The Role of Excess Vacancies on Precipitation Kinetics in an Al-Mg-Sc Alloy

F. FAZELI, C.W. SINCLAIR, and T. BASTOW

Recent studies using classical precipitation models to follow experimental precipitation kinetics in Al-Sc alloys have concluded that an explicitly time- and temperature-dependant interfacial energy must be adopted to explain the observed precipitation kinetics. An alternative explanation for the precipitation kinetics based on vacancy-enhanced diffusivity is proposed in this work. This method, combined with a classical Kampmann–Wagner (KWN) class model, has allowed us to reconcile the kinetics of nucleation, growth, and coarsening in an Al-Mg-Sc alloy using a single value for the interfacial energy in the temperature range 250 °C to 350 °C.

DOI: 10.1007/s11661-008-9587-1

I. INTRODUCTION

RESEARCH on Al-Sc alloys has been driven both by their potential as commercial age-hardenable alloys[1–3] as well by several characteristics that make them ''ideal'' for comparing against models of precipitation kinetics.[4–7] The desirable properties, in both these cases, arise from the presence of a high density of fine, approximately spherical Al_3Sc precipitates that resist coarsening or dissolution up to intermediate homologous temperatures.[3] Such precipitates are nearly ideal for pinning of grain boundaries and, thus, for achieving thermally stable, fine-grained microstructures.[8,9] From a fundamental point of view, these same properties make such alloys ideal for testing theories of precipitation given that many of the simplifying assumptions used in current models (*e.g.*, spherical geometry, dilute volume fraction, and ''homogeneous'' nucleation) are all approximately satisfied by this system.

One interesting feature arising from recent comparisons between experiment and classical kinetic models of nucleation, growth, and coarsening in Al-Sc alloys is that the experiments and models cannot be reconciled by use of a single value of the interfacial energy $\gamma_{Al/Al3Sc}$. It has been found that, in order to explain experimental results, the interfacial energy must be made a function of temperature or precipitate size. For an Al-0.11 at. pct Sc alloy, Hyland[4] reported that the value of $\gamma_{Al/Al3Sc}$ required to predict the incubation time for homogeneous nucleation based on classical nucleation theory was much smaller than that needed to replicate the steady-state nucleation rate. In the former case, the interfacial energy was estimated as 93 mJm^{-2}, while the interfacial energy of the latter was required to be 125 mJm^{-2}. Moreover, it was found, based on the measured incubation time, that the temperature dependence of the interfacial energy was required to increase from 78 mJm^{-2} at 561 K to 93 mJm^{-2} at 616 K.

Another example of this behavior can be found in the work of Robson *et al.*[5] In this case, an *N*-site model based on the Kampmann–Wagner (KWN) approach,[10] previously applied to a wide range of alloys (*e.g.*, References 11 and 12), was used to describe the precipitation in an Al-0.25 wt pct Sc alloy. In the KWN model, classical nucleation is applied, while growth is described based on diffusional growth of a spherical precipitate. The transitions from nucleation to growth, growth to coarsening, and the process of coarsening itself are implicitly accounted for due to the fact that a precipitate size distribution is followed throughout the process. Applying this framework to experimentally measured Al_3Sc size distributions in the Al-Sc system, Robson *et al.*[5] found that a much smaller value of the interfacial energy was needed for the initial stages of nucleation (57 mJm^{-2}) compared to that needed for describing coarsening of precipitates larger than 5 nm (200 mJm^{-2}). Robson reconciled this observation by arguing that the interfaces of the small nuclei would have greater ability to rearrange to lower their energy compared to much larger, coarsened precipitates. This is despite the fact that the precipitates were observed to remain coherent beyond a size of 5 nm. To fit their experimental results, a linear increase of the interfacial energy from 57 to 200 mJm^{-2}, saturating at a size of 5 nm, was used and found to give good agreement with the experimentally determined size distributions.

Several arguments may be given to explain why one might expect a temperature-/time-/size-dependent interfacial energy in the case of Al_3Sc precipitates. From a purely theoretical point of view, the interfacial energy as a thermodynamic property is temperature dependent, the temperature dependence being given by the entropy of the interface. For a sharp, coherent interface between Al and highly ordered Al_3Sc phase, the entropy contribution to the excess energy associated with the interface is quite small. Atomistic simulations on the binary Al-Sc

F. FAZELI, Postdoctoral Fellow, and C.W. SINCLAIR, Assistant Professor, are with the Department of Materials Engineering, The University of British Columbia, Vancouver, BC, Canada V6T 1Z4. Contact e-mail: ffazeli@interchange.ubc.ca T. BASTOW, Research Scientist, is with CSIRO, Division of Manufacturing and Infrastructure Technology, South Clayton MDC, Clayton, Vic. 3169, Australia.

Manuscript submitted August 1, 2007.
Article published online July 16, 2008

system indicate that a temperature increase from 400 to 800 K gives rise to only a 10 pct decrease in the calculated interfacial energy.[13] Alternatively, one could attribute modifications of interfacial energy to a modification of the interface itself at different temperatures or times, as was done by Robson. An obvious case would be the change in interfacial energy attending the transition from coherent to incoherent interfaces at a critical size.[7] In the case of Al-Sc alloys, however, this is only relevant to coarsening because the transition occurs for precipitate sizes >30 nm.[7] Other mechanisms that could be important in this context include segregation of solute to the interface. In the case of Al-Sc systems, recent atom probe measurements suggest that Mg may segregate to Al_3Sc interfaces.[14] While it has been argued that this will result in a reduction of interfacial energy compared with binary Al-Sc alloys, the effect is approximately time invariant and, as will be shown here, results in a small change in interfacial energy relative to the variations reported in the literature. In contrast, Ti can be gradually incorporated into Al_3Sc precipitates. While this too might be expected to provide a plausible explanation for a varying interfacial energy with time and temperature, Ti incorporation has been shown to only be significant after very long aging times.[15,16] This is attributable to the very low diffusivity of Ti in Al compared to Sc and means that significant effects would not be expected until after $\sim 10^2$ hours at 300 °C.[16] Finally, the back-calculated interfacial energies arising from the modeling described previously may only represent apparent energies and may, in fact, incorporate the effects of other distinct processes that are not included in the classic formulations described previously. The presence of intermediate precipitating phases, nonuniform solute concentrations, and excess vacancies all represent features that could affect the apparent interfacial energy.

In this work, we examine the possibility that excess vacancies could be responsible for the apparent variations in interfacial energy. First, experimental observations on the precipitation kinetics and precipitate size distribution in an Al-Mg-Sc-Ti alloy are presented. Next, these results are compared against predictions of a KWN model. Finally, the role that excess vacancies might play in this process is presented along with experimental evidence for their existence in the Al-Mg-Sc-Ti system studied here.

II. EXPERIMENTS

Materials were supplied by the Novelis Global Technology Centre (Kingston, ON) in the form of hot-rolled sheets 5-mm thick. These sheets were produced from laboratory castings made from high-purity Al and an Al-2 at. pct Sc master alloy resulting in an alloy with 2.8 wt pct Mg, 0.16 wt pct Sc, and a small amount of Ti. The Ti present in the alloy came both from Ti in the master alloy as well as additions made for grain refinement during laboratory casting. The hot-rolled sheet was found to have a coarse, unrecrystallized microstructure. In order to refine the microstructure and remove segregation, the hot-rolled sheet was subjected first to a homogenization treatment for 7 days at 610 °C in air followed by water quenching and cold rolling to 80 pct reduction. The cold-rolled sheet was subsequently annealed in a 40 pct $NaNO_3$ + 60 pct KNO_3 salt bath at 600 °C for 5 seconds and water quenched. The result of this heat treatment was a solutionized and recrystallized sample (confirmed by transmission electron microscopy) with an average grain size of approximately 50 μm. Aging treatments were carried out immediately following quenching from 600 °C, the precipitation reactions being performed at temperatures of 250 °C, 300 °C, or 350 °C. Based on previous work,[4,5] it was expected that at these low aging temperatures, where the undercooling below the equilibrium solvus temperature (*i.e.* 575 °C) is sufficiently high, homogenous nucleation would dominate. Several samples were aged for 8.5 hours at 300 °C and then up-quenched to 425 °C to accelerate coarsening. A temperature of 425 °C was determined as a compromise between obtaining fast kinetics and minimizing the change in equilibrium volume fraction of Al_3Sc, the change being estimated to be small (approximately 10 pct) due a very steep α-Al/α-Al + Al_3Sc solvus boundary.

The goal of these experiments was to compare the results against the KWN precipitation model. Two forms of measurement were made to facilitate this comparison. First, electrical conductivity was measured on various samples to capture its evolution with isothermal precipitation. Measurements were made at room temperature using a portable Verimet M4900C Eddy current reader operating in temperature-compensated mode to account for variations in ambient temperature. Assuming a linear relationship between conductivity and solute in solution, the conductivity measurements allow one to track the progress of precipitation by monitoring the depletion of solute in the aluminum matrix.

Precipitate size distributions measured at different aging conditions represent the second experimental measurements made for comparison against the KWN model. Samples for transmission electron microscopy were prepared from aged materials by punching 3-mm-diameter disks and mechanical polishing to a thickness of approximately 100 μm. These samples were finally jet polished in a 5 pct perchloric acid in methanol solution at -20 °C and a voltage of 20 V. Dark-field images using the $\langle 100 \rangle$ superlattice reflection of the Al_3Sc precipitates were taken at different magnifications depending on aging condition using a Hitachi H-800 scanning transmission electron microscope operating in conventional mode at 200 KV. Digital image analysis was used to determine the diameter of the Al_3Sc precipitates from these dark-field images. In each case, a minimum of 10^3 precipitates were measured to construct the size distributions.

Finally, high field nuclear magnetic resonance (NMR) spectroscopy was used to confirm a number of basic aspects of the precipitation in this system. The NMR is particularly useful for following precipitation in dilute Al-Sc alloys due to a high detection sensitivity for the ^{45}Sc nucleus and a significant difference in the Knight shift (600 ppm) between the ^{45}Sc spectra for Sc in solid

solution and Sc in the Al_3Sc phase. In this study, samples were analyzed for one aging temperature to confirm the onset and end of precipitation and the absence of other intermediate precipitates. For this purpose, a Bruker MSL 400 NMR spectrometer with a nominal 9.395T field and an observation frequency of 97.2 MHz was used. A scan rate of 10 Hz was used to collect the spectra, which each contained approximately 5×10^5 scans. The portion of the spectra corresponding to the locations of the Al matrix (1700 ppm) and Al_3Sc phase (1040 ppm) are shown here. Prior to analysis, homogenized material was filed into a powder (size of granules was approximately 160 μm) followed by annealing at 610 °C for 1 minute. The powder was encapsulated in a quartz tube that had been evacuated and backfilled with approximately 0.33 atm of Ar. After 1 minute, this quartz tube was shattered into an ice water bath. Four different lots of the powder were then annealed at 350 °C for 0 seconds (as solutionized), 10 minutes, 30 minutes, 1 hour, and 2 hours, respectively.

III. EXPERIMENTAL RESULTS

The results of electrical resistivity measurements made on samples aged isothermally at 250 °C, 300 °C, or 350 °C for various times are shown in Figure 1. In previous studies, the electrical resistivity has been used to directly calculate the volume fraction of precipitates in Al-Sc alloys assuming scattering dominated by solute in the aluminum matrix (*e.g.*, Reference 17). As will be discussed later, care must be exercised in making this relation as it may not be possible to ignore the contribution of interfacial scattering to the measured resistivity. In the present case, the relative change in resistivity is used as an approximate tool for following the precipitation kinetics and, in particular, for identifying the start and end times for precipitation. The appropriateness of the values obtained for the precipitation start time have been corroborated by comparing the values obtained from resistivity *vs* those obtained by observing the aging response of the alloy.

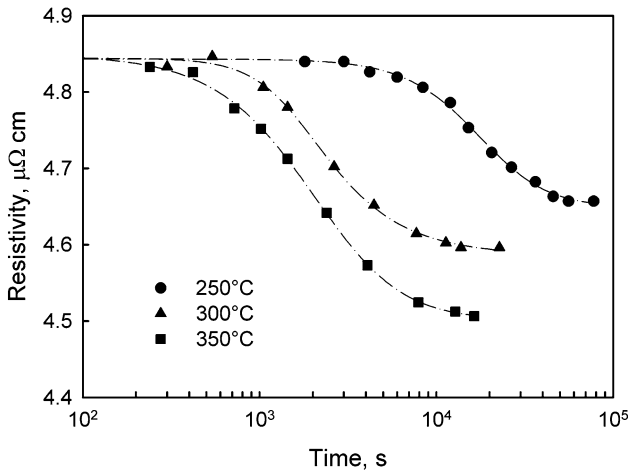

Fig. 1—Evolution of resistivity during aging at different temperatures.

The NMR spectra (Figure 2) made on samples aged at 350 °C for times up to 2 hours show two noteworthy features. First, the spectra from the solutionized sample indicate the absence of a peak corresponding to Al_3Sc at 1040 ppm, thus confirming that the solutionization treatment was adequate. Second, the NMR spectra show no evidence of other Sc containing phases, confirming the expected result that the Al_3Sc forms directly without intermediate precipitates. It should be noted that compared to binary Al-Sc alloys,[18] the Al_3Sc peaks observed here on aging at 350 °C exhibited extensive and symmetric wings due either to imperfectly formed Al_3Sc crystallites or to Mg proximity. Finally, it is worth noting that the precipitation start and finish times estimated from resistivity are consistent with the observed appearance of the Al_3Sc peak in the NMR spectra and the relatively small change in this peak for measurements between 1 and 2 hours.

Given that the KWN model directly tracks the precipitate size distribution on aging, measurements of the size distributions give a second experimental measurement that can be compared with the model.

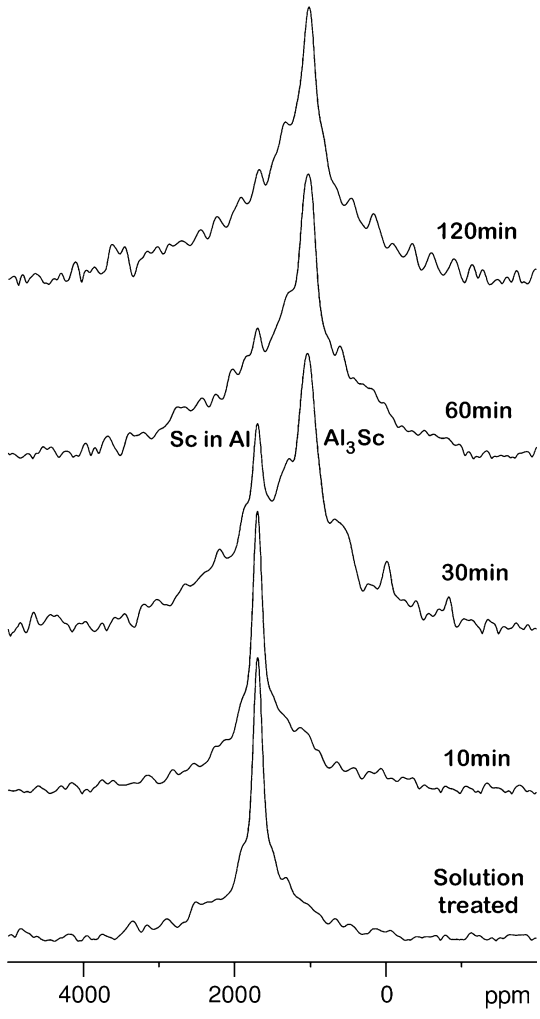

Fig. 2—Evolution of NMR spectra for ^{45}Sc nucleus in the solution (at 1700 ppm) and in the Al_3Sc phase (at 1040 ppm) for different stages of aging at 350 °C.

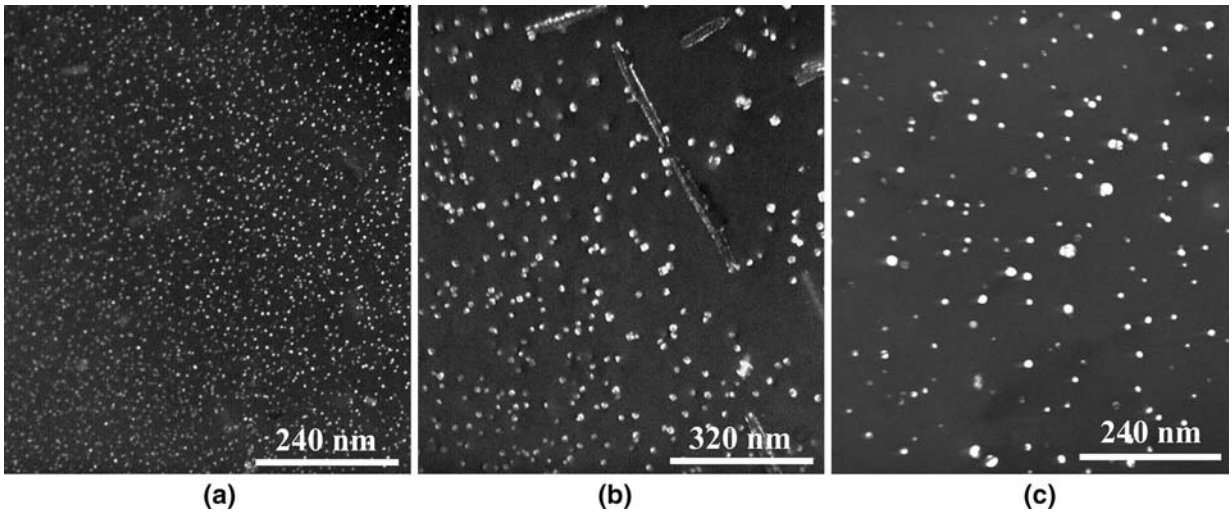

Fig. 3—Dark-field TEM images using the reflection of Al_3Sc fcc-$L1_2$ phase showing different populations of the particles resulted from aging treatment: (*a*) 2.5 h at 300 °C, (*b*) 2 h at 350 °C, and (*c*) 8.5 h at 300 °C followed by 80 minutes coarsening at 425 °C. The low density of rods/laths observed in (b) are likely a second morphology of Al_3Sc observed under conditions of low supersaturation (*e.g.*, References 16 and 19).

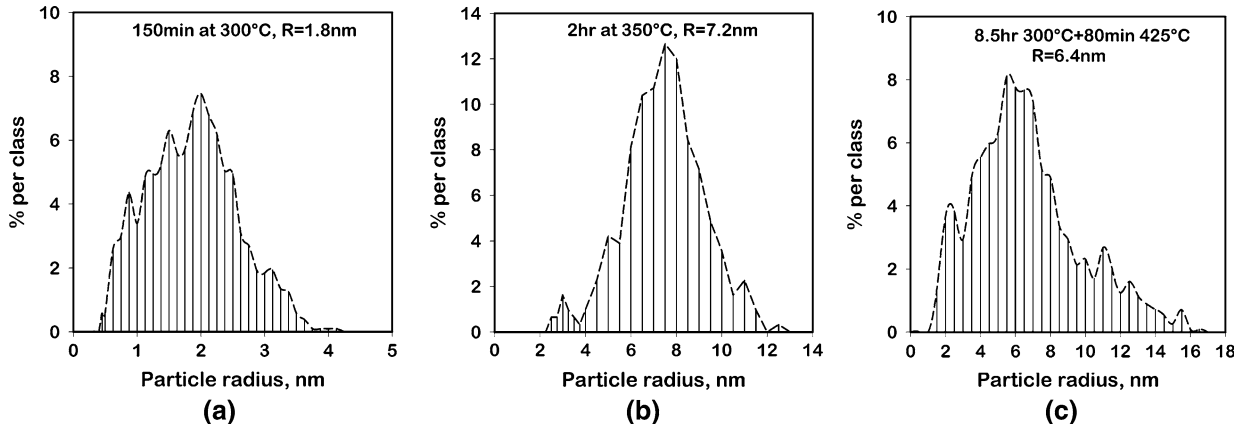

Fig. 4—Measured size distribution of Al_3Sc precipitates at three aging conditions: (*a*) one-step aging at 300 °C for 2.5 h, (*b*) one-step aging at 350 °C for 2 h, and (*c*) two-step aging, *i.e.*, 8.5 h aging at 300 °C followed by 80 min holding at 425 °C to enhance coarsening.

Figures 3 and 4 give examples of dark-field TEM images and the corresponding size measurements, respectively, made under the three indicated aging conditions. As is generally observed,[19] the Al_3Sc remain equiaxed over all the aging conditions examined. Moreover, bright-field imaging shows Ashby–Brown contrast consistent with coherence for all aging conditions.

IV. MODELING

The KWN model[10] has been previously applied to Al-Sc binary alloys by Robson *et al.*,[5] where it was shown that a precipitate-size-dependent interfacial energy had to be used to capture the precipitation kinetics in an Al-Sc alloy. We use this as a starting point to show that a similar situation exists when this model is applied to our Al-Mg-Sc-Ti alloy. It will finally be shown that this temperature/size dependence can be fully removed if the KWN model is adapted to account for the effect of excess vacancies.

A. *Modeling Approach: KWN Model*

To simplify, we consider that Al and Sc are the only species to participate in the precipitation reaction, *i.e.*, that neither magnesium nor titanium is incorporated into the precipitates. This assumption can be refined, as will be discussed subsequently, given that magnesium is incorporated to a small extent on the Al sublattice, while Ti tends to incorporate with increasing strength at long times on the Sc sublattice.[15]

The size distribution of precipitates has been discretized into a finite number of size classes. The temporal evolution of the number of precipitates in each of these classes has been calculated based on a constant time increment. To be able to accurately track the evolution of both the large and small ends of the size distribution with equal accuracy, a logarithmic division of size has been used to generate 300 class sizes, where the radius of the *i*th class (measured in nanometers) is given by

$$\log\ (R_i) = -9.5 + \frac{i}{100} \quad \text{for } i = 0 \text{ to } 300 \qquad [1]$$

As in the case of Robson *et al.*, we have adopted classical nucleation to calculate the number of new nuclei arriving in the size classes over each time interval. In support of this approach, recent comparisons between the predictions of classical nucleation *vs* cluster dynamics show that the classical formulation works well for the case of Al_3Sc precipitation.[20] The nucleation rate is thus given by

$$\dot{N} = Z\beta^* N_V \exp\left(\frac{-\alpha\gamma^3}{k_B T(\Delta G_V)^2}\right) \exp\left(\frac{-\tau}{t}\right) \qquad [2]$$

where Z is the Zeldovich nonequilibrium factor (approximated as 0.05), β^* is the attachment rate of single atoms to the critical nucleus, N_V is the number of atoms per unit volume, ΔG_V is the driving pressure for nucleation, α is a constant, and γ represents the interfacial energy. The incubation time, τ, is taken here as $(2Z\beta^*)^{-1}$. The parameter β^* is related to the size of critical nucleus, the diffusivity of solute, and the solute content of Al matrix.

While Robson *et al.* incorporated the possibility of heterogeneous nucleation on dislocations at high aging temperatures in their model, here only homogeneous nucleation, consistent with our TEM observations, is dealt with. Due to our choice of low aging temperatures, the elastic energy contribution to the total energy change associated with precipitation appears to be negligible and, thus, is neglected. Based on the fact that Sc is a dilute alloying species, we approximate the chemical driving force as[21]

$$\Delta G_V = \frac{R_g T}{V_m}\left[X_{\text{Sc}}^{\text{Al3Sc}} \ln \frac{X_{\text{Sc}}(t)}{X_{eq}} + (1 - X_{\text{Sc}}^{\text{Al3Sc}}) \ln \frac{1 - X_{\text{Sc}}(t)}{1 - X_{eq}}\right] \qquad [3]$$

where V_m is the molar volume; and $X_{\text{Sc}}^{\text{Al3Sc}}$, X_{Sc}, and X_{eq} are the atomic fraction of Sc in the precipitate, the actual content in the matrix, and the equilibrium fraction in the matrix.

The growth rate of the precipitates is considered to be governed by the diffusional growth of spherical precipitates. The diffusivity of Sc in Al is from the work of Fujikawa[22] and has been shown to work well for Al-Mg-Sc ternary alloys.[23] The pre-exponential factor is 5.31×10^{-3} m^2/s, and the activation energy is 174 kJ/mol. The off-diagonal terms of the diffusivity tensor are not considered here. The solute remaining in solution is calculated at the end of each step using a mean-field approximation based on a mass balance of the solute within the precipitate size distribution. The solubility of the precipitates as a function of their size, X_R, is corrected for the Gibbs–Thompson effect:

$$X_R = X_{eq} \exp\left(\frac{V_m}{R_g T}\frac{2\gamma}{R}\frac{(1 - X_{eq})}{(X_{\text{Sc}}^{\text{Al3Sc}} - X_{eq})}\right) \qquad [4]$$

Those precipitates with X_R larger than X_{Sc} are unstable and will dissolve. Once the size of a group of precipitates approached the lower tail of the distribution, they were removed permanently from the system. In this way, the coarsening is explicitly taken into account and no *a priori* assumption regarding its commencement needs to be made.

The equilibrium solubility required in Eqs. [3] and [4] is based on knowledge of the thermodynamics for the quaternary system under study here (Al-Mg-Sc-Ti). The influence of a small amount of Ti in solution on the solubility of Sc is expected to be low, because most of the Ti is tied up as intermetallic inclusions. The effect of having 2.8 at. pct Mg in solution also tends to have only a small effect on the solubility of Sc in Al for temperatures below 400 °C.[24] Based on these and by virtue of the fact that the limited published thermochemistry data does not capture the complex nature of the binary/ternary interactions of these solutes in Al, the solubility of Sc in Al has been evaluated by accounting only for the effect of 2.8 wt pct Mg in solution. The solubility used in the simulations is calculated based on the thermodynamic data of Grobner *et al.*[25] and is defined by the entropy and enthalpy of Sc in solution as 63.8 J/mol K and 66.9 kJ/mol, respectively. At low temperatures, this solvus is very close to that of a binary Al-Sc alloy.[17]

B. *Comparison between KWN Model and Experiment: the Role of Excess Vacancies*

As a starting point for comparing the KWN model described previously to the experimental kinetics of precipitation in the Al-Mg-Sc-Ti system, we have estimated the incubation time for precipitation at the three temperatures studied by fitting to the resistivity data (*cf.* Figure 1) and finding the time for 10 pct change in resistivity. These data are shown in Figure 5. The KWN model was fit to these data (Table I) using the interfacial energy as the only adjustable parameter. If a constant interfacial energy is used regardless of precipitation time/temperature, then the model

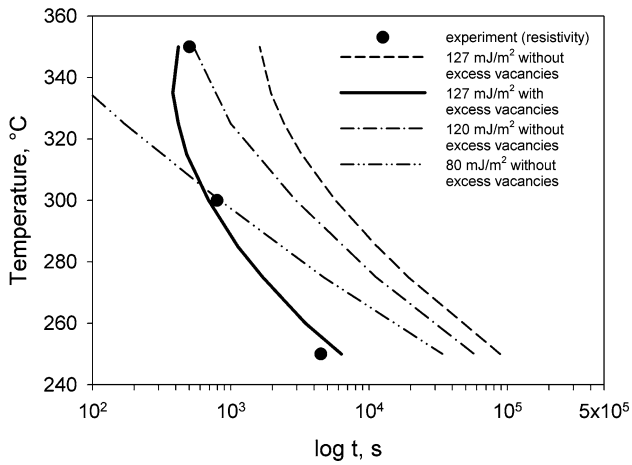

Fig. 5—Time for 10 pct of precipitation at different aging temperatures. The measurements (solid circles) are based on the resistivity test (summarized in Table I), and the lines represent the model predictions.

Table I. Isothermal Aging Time Required for 10 Pct Precipitation of Al_3Sc Based on Conductivity Measurements

T, °C	250	300	350
$T_{10\ pct}$, s	4467	795	501

underpredicts the kinetics at high temperature and overpredicts them at low temperatures. This is the same trend as observed by Hyland.[4] The experimental results can be reconciled with the model if a temperature-dependent interfacial energy is chosen. Allowing for this variation would predict interfacial energies of 80 and 120 mJm^{-2} at 300 °C and 350 °C, respectively. At the highest aging temperature, *i.e.*, 350 °C, the predicted incubation time is quite sensitive to the value assumed for the interfacial energy. In contrast, for 250 °C, the calculated incubation time has weak interfacial energy dependence such that the experimental value cannot be captured by the model using the interfacial energy as a sole fit parameter.

Segregation of Mg to Al_3Sc interfaces has been observed using the three-dimensional–tomographic atom probe by Marquis *et al.*[14] This segregation leads to a reduction in the interfacial energy with Mg coverage of the interface. Adopting the data from this work allows us to estimate the Gibbs interfacial excess Mg (Γ_{Mg}) for our alloy. From these data, we estimate the Mg coverage as 2.4 and 1.6 atom nm^{-2} for aging at 250 °C and 300 °C. These values reduce the interfacial energy by 17 and 12 mJm^{-2}, respectively, compared to the interfacial energy of the precipitates in a binary Al-Sc alloy. As is apparent, from Figure 5, particularly from aging at 250 °C, the change in interfacial energy predicted previously is insufficient to explain the differences observed here. Moreover, as will be shown subsequently, much larger changes would be required to describe the overall kinetics, particularly at 250 °C.

The question that arises is whether there is another unaccounted mechanism missing from the KWN model described previously that could be giving rise to the apparent temperature dependence of the interfacial energy. In making TEM observations, it was observed that all grains exhibited precipitate-free zones (PFZ) around the grain boundaries, as illustrated in Figure 6. The presence of PFZs in aluminum alloys is often taken as an indication that either vacancies are playing a role in precipitation or that solute depletion due to grain boundary precipitation is locally reducing supersaturation.[26,27]

Solute depletion due to the precipitation on boundaries such as that observed in Figure 6 cannot be solely responsible for the observed PFZ. A simple calculation of the diffusion distance for Sc, $\sqrt{D_{Sc}^{Al}t}$, gives 0.45 μm for the aging conditions in Figure 6. This is to be contrasted with the width of the PFZs, which appears to be 2 μm on either side of the grain boundary. Thus, one must consider the possibility that vacancies participate in the progress of precipitation.

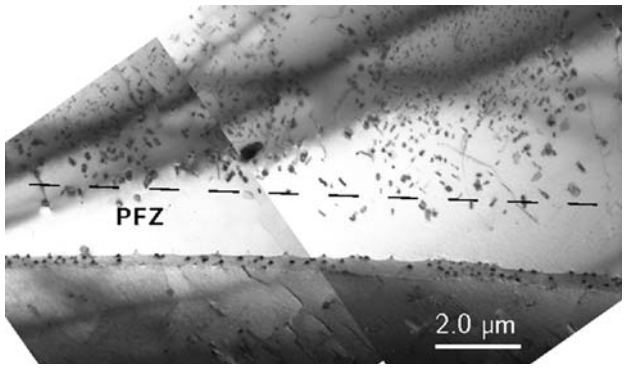

Fig. 6—Bright-field TEM image showing a PFZ in the vicinity of a grain boundary. Aging treatment: 3 h at 400 °C.

The heterogeneous precipitation of Al_3Sc at vacancy clusters appears unlikely as an explanation for the PFZ observed here, because the measured maximum number density of the precipitates has been found to remain invariant in the presence of excess vacancies.[4] This is likely a consequence of the high binding energy between Sc atoms and vacancies, $Q_b = 0.35$ eV,[28] which prevents the condensation of excess vacancies into clusters. Moreover, because vacancies are neither created nor destroyed at coherent boundaries (such as those of the Al_3Sc precipitates studied here), the activation energy for homogeneous nucleation of Al_3Sc precipitates will not be affected by excess of vacancies. The remaining effect that can be attributed to the presence of excess vacancies is enhanced Sc diffusivity. Such an effect would explain the apparent reduction in incubation times, particularly at low temperatures observed in Figure 5 as well as by Hyland.[4]

To account for the effect of excess vacancies on diffusivity, a simple model is proposed here. An effective diffusivity is taken as

$$D_{\text{eff}} = D_{\text{Sc}}\left(1 + \frac{X^{\text{exc}}}{X_V^{eq}}\right) \qquad [5]$$

where X^{exc} is the concentration of excess vacancies (*i.e.*, the total vacancy concentration minus the equilibrium concentration) and X_V^{eq} is the equilibrium concentration of vacancies. Alloying aluminum with Sc has also been shown to decrease the activation enthalpy for vacancy formation, thereby increasing the concentration of excess vacancies expected on quenching.[28] The concentration of excess vacancies on quenching in binary Al-Sc alloys has been given as[28]

$$\frac{X^{\text{exc}}}{X_V^{eq}} = \frac{(1 - zX_{Sc})\exp\left(-Q_V/\text{k}T_{\text{sol}}\right) + zX_{Sc}\exp\left[-(Q_V - Q_b)/\text{k}T_{\text{sol}}\right]}{(1 - zX_{Sc})\ \exp\ \left(-Q_V/\text{k}T_{\text{age}}\right) + zX_{Sc}\ \exp\ \left[-(Q_V - Q_b)/\text{k}T_{\text{age}}\right]} - 1 \qquad [6]$$

where z is the number of neighboring atoms (12 in the fcc lattice), Q_v is the activation energy for vacancy formation in pure Al, and T_{sol} and T_{age} are the solution treatment and aging temperatures, respectively.

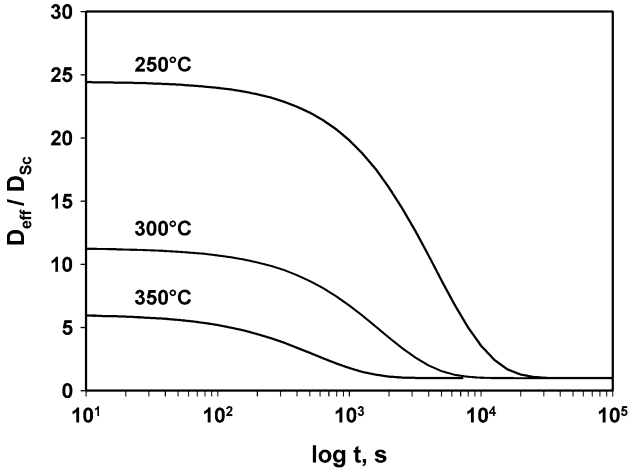

Fig. 7—Variation of D_{eff}/D_{Sc} ratio with time, indicating the temporal decay of excess vacancies for different aging temperatures. For the calculation, D_{Vo}/L^2 = 1.0 ks^{-1}, together with the activation energy data depicted in Table II, was used.

Table II. Some Model Parameters Used in the Precipitation Model

Parameter	Value	Comment
N_V	6.07 × 10^{28}, m^{-3}	
Q_m	68.8, kJ/mol	Q_{SD}–Q_V
Q_{SD}	142, kJ/mol	Ref. 31
D_o^{Al}	1.7 × 10^{-4}, m^2/s	Ref. 31
Q_V	73.2, kJ/mol	Ref. 32
S_V	20, J/mol K	Ref. 32
V_m	9.9 × 10^{-6}, m^3/mol	
Z	12	

On aging, the concentration of excess vacancies will tend to decay, leading to a time-dependent effective diffusivity that approaches D_{Sc} at long aging times. Here, we take a simple exponential decay of the excess vacancy concentration assuming that annihilation of vacancies will tend to occur at other defects such as grain boundaries and dislocations.[29] This gives

$$X^{exc}(t) = X_o^{exc} \exp\left(-t\frac{D_V}{L^2}\right) \quad [7]$$

Here, D_v is the diffusivity for vacancies in aluminum with activation energy of Q_m and D_{vo} as a pre-exponential factor, and L is a characteristic annihilation distance for vacancies. The activation energy for vacancy diffusion (Q_m) is approximated as the difference between the activation energy for self-diffusion of Al and the activation energy for vacancy formation. The pre-exponential term for the vacancy diffusivity is more difficult to identify, as is the characteristic annihilation distance, L. Without having a solid foundation for the term D_{vo}/L^2, it is used here as a fitting parameter in the model.

Returning to the data first presented in Figure 5, we have been able to obtain excellent agreement between the KWN model, accounting for the effect of excess vacancies on diffusivity with the incubation time in the range of 250 °C and 350 °C using a single value for the interfacial energy ($\gamma_{Al/Al3Sc}$ = 127 mJm^{-2}) and a value of D_{vo}/L^2 = 1.0 ks^{-1}. One can see the effect of the excess vacancies on the diffusivity of Sc, in terms of D_{eff}/D_{Sc}, in Figure 7. Here, it is shown that the effect is strongest, and persists longest, at low temperatures. This is consistent with our preceding observation that the classical model (without excess vacancies) is poorest at capturing the experimental behavior at low temperatures.

The preceding interfacial energy is within the range reported for Al_3Sc/Al interphase coherent boundaries[30] and is consistent with the value calculated by Hyland.[4] The value used for D_{vo}/L^2, though here used purely as a

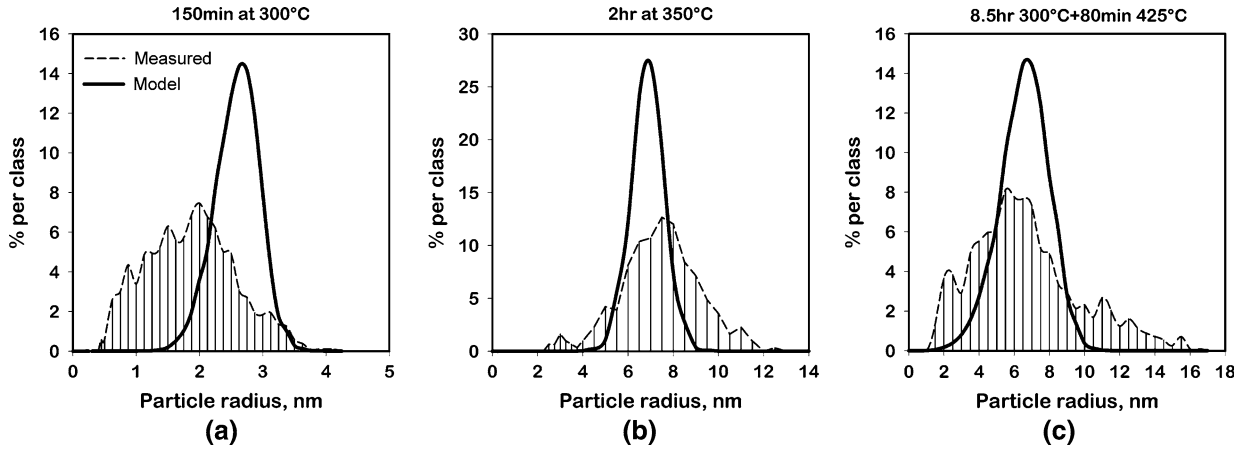

Fig. 8—Comparison of the measured size distribution of Al_3Sc precipitates with that of predicted by the model for three aging conditions: (*a*) one-step aging at 300 °C for 2.5 h, (*b*) one-step aging at 350 °C for 2 h, and (*c*) two-step aging, *i.e.*, 8.5 h aging at 300 °C followed by 80 min holding at 425 °C to boost coarsening.

fitting parameter, is physical and, thus, can be checked against a simple estimate. A value for D_{vo} can be estimated from

$$D_{Vo} \approx \frac{D_o^{\mathrm{Al}}}{\exp\ (S_V/R_g)} \qquad [8]$$

where values for the pre-exponential factor for aluminum self-diffusion D_o^{Al} and entropy of vacancy formation S_v are given in Table II. Estimating the annihilation distance as the grain size ($d = 50\ \mu$m) gives $D_{Vo} = 6.1\ \mathrm{ks}^{-1}$, which is a factor of 6 higher than that obtained from fitting experimental data. There are several possible explanations for this overestimation. First, the entropy of vacancy formation is taken for pure aluminum and is likely modified in the presence of Sc. The annihilation distance may also be significantly underestimated, particularly if one considers that, because of their strong binding energy, vacancies become trapped by Sc atoms for some period of time, thus causing them to have a longer random walk process.

The preceding comparisons were made purely based on the incubation time, *i.e.*, the initial stages of the precipitation. If the model is robust, it should also be capable of predicting the full precipitation kinetics using the same parameters. Figure 8 shows the comparison between measured and calculated precipitate size distributions. The model captures the size distribution reasonably well, though it does tend to underpredict the width of the distribution, a feature that has been previously reported for KWN models,[12] and slightly underpredicts the mean precipitate size for aging at 300 °C. Importantly, the model is able to capture the size distributions obtained under isothermal aging conditions, as well as those obtained for samples that were up-quenched from 300 °C to 425 °C.

As a final confirmation of the robustness of the model, the overall kinetics of precipitation as estimated from resistivity measurements can be compared against the model predictions. As noted previously, one must take care with attributing resistivity change solely to depletion of solute from solution. Other features can complicate the interpretation. An important but often overlooked contribution to resistivity in the case of finely spaced precipitates (spacing < 100 nm in aluminum alloys) is interfacial scattering from the precipitate interfaces.[33] In the current case, the precipitate spacing for all conditions is predicted to decrease rapidly with the onset of nucleation. For samples treated at 250 °C and 300 °C, it is observed that the spacing rapidly decreases to be less than 100 nm in the early stages of precipitation. Thus, while our earlier predictions of the precipitation start times (those used to create Figure 5) are not strongly affected by interfacial scattering, quantitative comparisons at longer aging times are less likely to be accurate.

Assuming that the resistivity change can be attributed entirely to the removal of Sc from solution, the predictions of the solute content in aluminum from the KWN model have been converted to a resistivity change using $\Delta\rho = 3.4\ \mu\Omega$/cm per Sc atomic percent.[34,35]

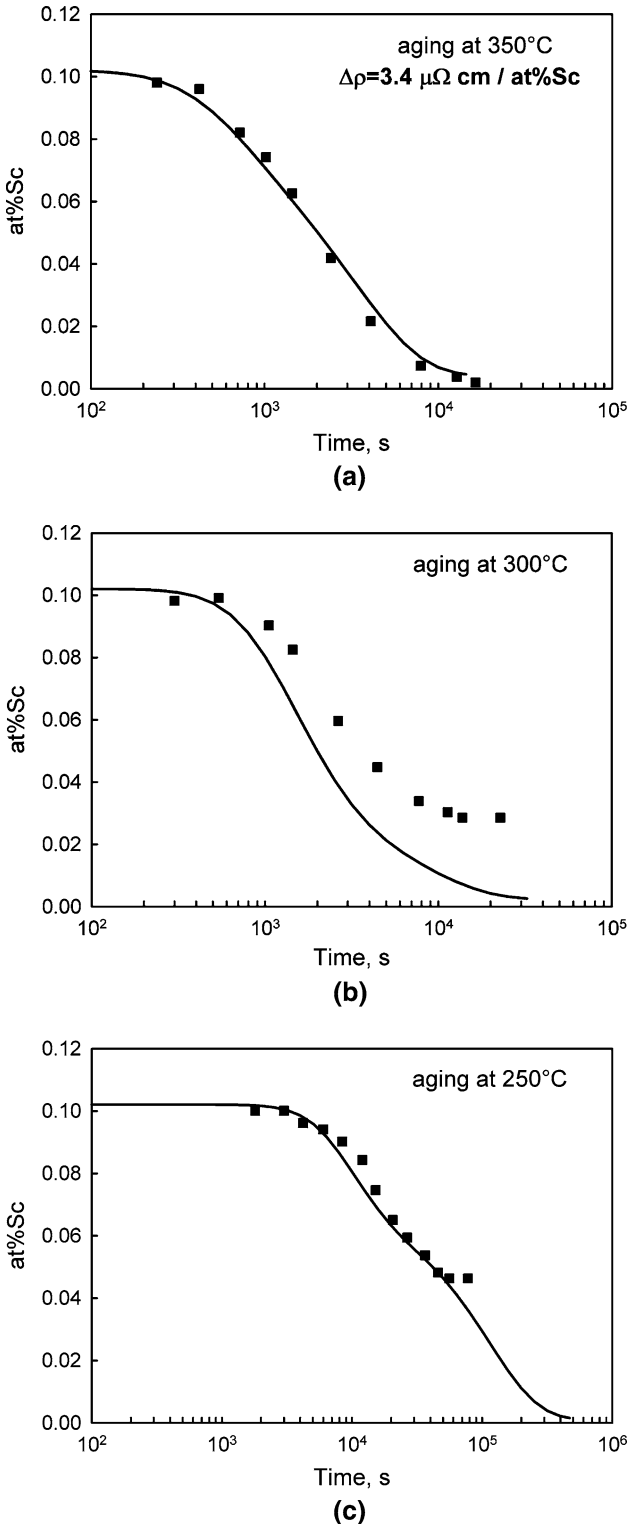

Fig. 9—Kinetics of precipitation quantified using resistivity measurements (symbols) compared with model predictions (line) for aging at 350 °C, 300 °C, and 250 °C.

There exists a large spread in values reported for this parameter in the literature (Reference 17), the value selected here being near the middle of the reported values. The calculated resistivity change from the model

is then compared directly against the measured resistivity change (Figure 9). As expected based on the preceding comments, the measured resistivity change appears to compare well to the model at early times. However, as precipitation nears completion at 250 °C and 300 °C, one observes that the experiments suggest a much higher solute remaining in solution compared to the model. On the other hand, at an aging temperature of 350 °C, where the precipitate spacing is expected (based on the KWN model) to remain greater than 100 nm throughout the precipitation sequence, the model prediction is found to be in excellent agreement with the experimental data.

V. CONCLUSIONS

The classic KWN model for precipitation has been modified to account for the effects of excess vacancies on the diffusivity in Al-Sc alloys. This effect is enhanced in Al-Sc alloys due to the strong binding energy between Sc and vacancies. This leads to an increased excess vacancy concentration compared with pure aluminum. This model predicts the precipitation kinetics and precipitate size distribution in both isothermal and nonisothermal treatments for the temperature range considered here using the *single* value for the interphase interfacial energy whose value is within the range previously reported. The proposed model requires only two adjustable parameters, comparable to the empirical temperature-/size-dependent interfacial energy models previously proposed. Further experimental work is required to establish the concentration of vacancies under different heat-treatment conditions, as well as to quantify their decay kinetics, and to test the proposed model against other Al-Sc–based alloys.

ACKNOWLEDGMENTS

The authors thank W.J. Poole (University of British Columbia) for detailed discussions on this work, X. Wang (McMaster University) for assistance with transmission electron microscopy, and C.R. Hutchinson and J. Da Costa Teixeira (Monash University) for comments on the manuscript. The financial support of the Natural Sciences and Engineering Research Council of Canada is gratefully acknowledged, as is the supply of materials for this study by Novelis.

REFERENCES

1. L.S. Toporova, D.G. Eskin, M.L. Kharakterova, and T.B. Dobatkina: *Advanced Aluminum Alloys Containing Scandium*, Gordon & Breach, Amsterdam, 1998.
2. N. Blake and M.A. Hopkins: *J. Mater. Sci.*, 1985, vol. 20, p. 2861.
3. N. Seidman, E.A. Marquis, and D.C. Dunand: *Acta Mater.*, 2002, vol. 50, pp. 4021–35.
4. R.W. Hyland: *Metall. Trans. A*, 1992, vol. 23A, pp. 1947–55.
5. J.D. Robson, M.J. Jones, and P.B. Prangnell: *Acta Mater.*, 2003, vol. 51, pp. 1453–68.
6. G.M. Novotny and A.J. Ardell: *Mater. Sci. Eng. A*, 2001, vol. 318, pp. 144–54.
7. S. Iwamura and Y. Miura: *Acta Mater.*, 2004, vol. 52, pp. 591–600.
8. M.J. Jones and F.J. Humphreys: *Acta Mater.*, 2003, vol. 51, pp. 2149–59.
9. Y.W. Riddle and T.H. Sanders: *Metall. Mater. Trans. A*, 2004, vol. 35A, pp. 341–50.
10. R. Wagner and R. Kampmann: *Mater. Sci. Technol.*, 1991, vol. 5, pp. 213–303.
11. R. Kampmann and R. Wagner: *Decomposition of Alloys: the Early Stages*, P. Hassen, ed., Pergamon, Oxford, United Kingdom, 1984, p. 91.
12. J. Yang and M. Enomoto: *ISIJ Int.*, 2005, vol. 45, pp. 1335–44.
13. R.W. Hyland, Jr., M. Asta, S.M. Foiles, and C.L. Rohrer: *Acta Mater.*, 1998, vol. 46, pp. 3667–78.
14. E.A. Marquis, D.N. Seidman, M. Asta, and C. Woodward: *Acta Mater.*, 2006, vol. 54, pp. 119–30.
15. C.B. Fuller, J.L. Murray, and D.N. Seidman: *Acta Mater.*, 2005, vol. 53, pp. 5401–13.
16. M.E. van Dalen, D.C. Dunand, and D.N. Seidman: *Acta Mater.*, 2005, vol. 53, pp. 4225–35.
17. J. Røyset and N. Ryum: *Mater. Sci. Eng. A*, 2005, vol. 396, pp. 409–22.
18. S. Celotto and T.J. Bastow: *Phil. Mag.*, 2000, vol. A80, pp. 1111–25.
19. E. Marquis and D.N. Seidman: *Acta Mater.*, 2001, vol. 49, pp. 1901–19.
20. E. Clouet, M. Nastar, A. Barbu, C. Sigli, and G. Martin: in *Solid-Solid Phase Transformations in Inorganic Materials 2005*, J.M. Howe, E.D. Laughlin, J.K. Lee, D.J. Srolovitz, and U. Dahmen, eds., TMS, Warrendale, PA, 2005, pp. 683–03.
21. H.I Aaronson, K.R. Kinsman, and K.C. Russell: *Scripta Metall.*, 1970, vol. 4, pp. 101–06.
22. S.I. Fujikawa: *Def. Diffus. Forum*, 1997, vols. 143–147, p. 115.
23. E. Marquis and D.N. Seidman: *Acta Mater.*, 2005, vol. 53, pp. 4259–68.
24. A. Pisch, J. Grobner, and R. Schmid-Fetzer: *Mater. Sci. Eng. A*, 2000, vol. 289, pp. 123–29.
25. J. Grobner, R. Schmid-Fetzer, A. Pisch, G. Cacciamani, P. Riani, N. Parodi, G. Borzone, A. Saccone, and R. Ferro: *Z. Metallkd.*, 1999, vol. 90, pp. 872–80.
26. P.C. Varley, M.K.B. Day, and A. Sendork: *J. Inst. Met.*, 1957–58, vol. 86, pp. 337–51.
27. J.D. Embury and R.B. Nicholson: *Acta Metall.*, 1965, vol. 13, pp. 403–17.
28. Y. Miura, C.H. Joh, and T. Katsube: *Mater. Sci. Forum*, 2000, vols. 331–337, pp. 1031–36.
29. P. Shewmon: *Diffusion in Solids*, 1st ed., McGraw-Hill, New York, NY, 1963, p. 76.
30. J. Royset and N. Ryum: *Int. Mater. Rev.*, 2005, vol. 50, pp. 19–44.
31. J. Frost and M.F. Ashby: *Deformation Mechanism Maps*, Pergamon, Oxford, United Kingdom, 1982.
32. J. Røyset and N. Ryum: *Scripta Mater.*, 2005, vol. 52, pp. 1275–79.
33. B. Raeisinia and W.J. Poole: *Mater. Sci. Eng. A*, 2006, vol. 420, pp. 245–49.
34. S.I. Fujikawa, M. Sugaya, H. Takei, and K.I. Hirano: *J. Less-Common Met.*, 1979, vol. 63, pp. 87–97.
35. H.-H. Jo and S.-I. Fujikawa: *Mater. Sci. Eng. A*, 1993, vol. 171, pp. 151–61.